

---

Soot production in high  
pressure inverse diffusion  
flames with enriched oxygen in  
the oxidizer stream

Supplementary Information

---

# Contents

|  |          |
|--|----------|
| <b>S1 Experimental details</b>                         | <b>2</b> |
| S1.1 Details of the burner . . . . .                   | 2        |
| S1.2 Details of the LII and LIF measurements . . . . . | 2        |
| S1.2.1 LII signal detection . . . . .                  | 3        |
| S1.2.2 Pressure effects on LII signals . . . . .       | 4        |
| S1.2.3 LIF signal selection . . . . .                  | 6        |
| <b>S2 Varying parameters in CoFlame</b>                | <b>7</b> |

## S1. Experimental details

### S1.1. Details of the burner

The burner and the experimental details are illustrated in Fig. S1.

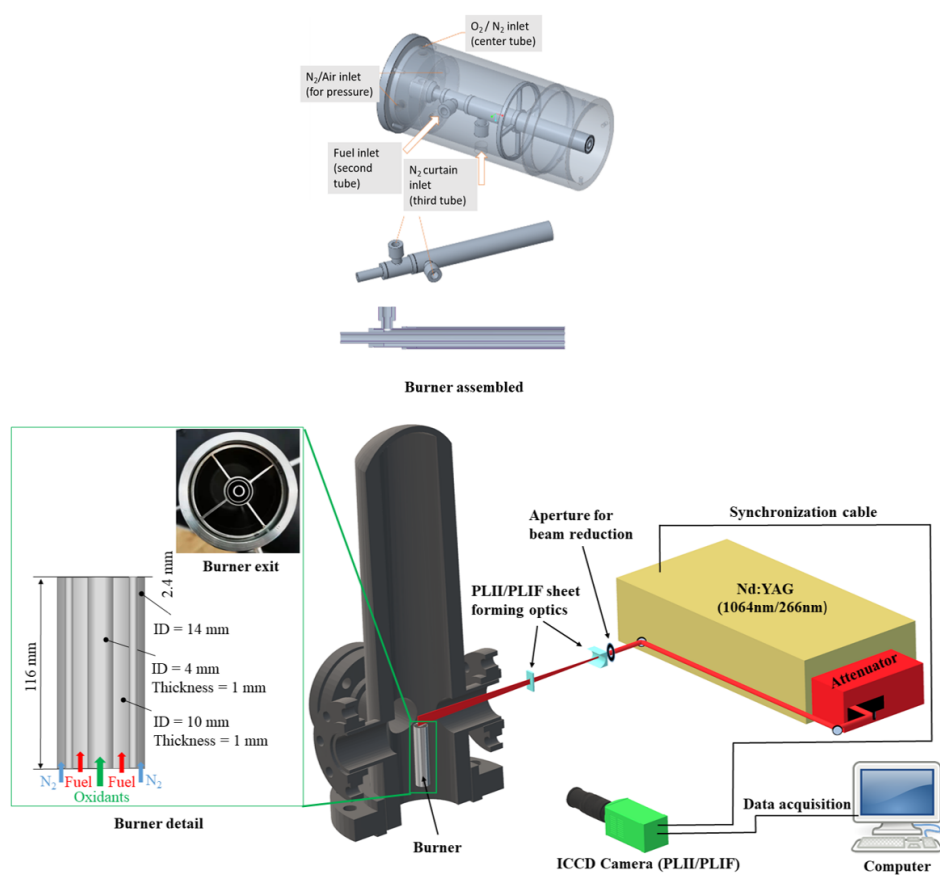


Figure S1: Experimental setup and burner details.

### S1.2. Details of the LII and LIF measurements

### *S1.2.1. LII signal detection*

The energy variation along the laser sheet height was monitored by a power meter operating in an averaging mode, and was less than 20%. Energy profile correction was not carried out for the captured LII signal, since the measurements were conducted at the plateau region of a laser fluence curve with a fluence of  $0.35 \text{ J/cm}^2$  as presented in Fig. S2. The signal was captured by an ICCD camera (PI-MAX3l  $1024 \times 1024$ ) with the gate time 100 ns and with a  $435 \pm 40 \text{ nm}$  bandpass filter (Semrock). All captured LII signals were within the linear region of the ICCD, the upper limit of which was around 9400 counts as shown in Fig. S3. The saturation limit of the ICCD was 60000 counts.

The effect of varying the gate time was also assessed and was presented in Fig. S4. It is shown that the effect was mild, as the linearity of the LII signals with pressure remained. Thus, varying the gate time would not change the conclusions of this study.

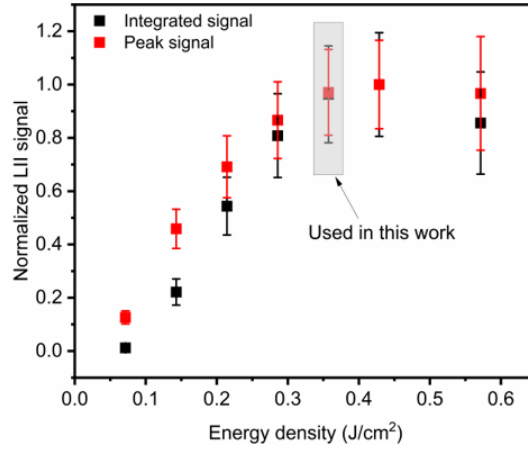


Figure S2: LII signal with different laser energies. The test flame is F-70%-O<sub>2</sub> at 5 bar.

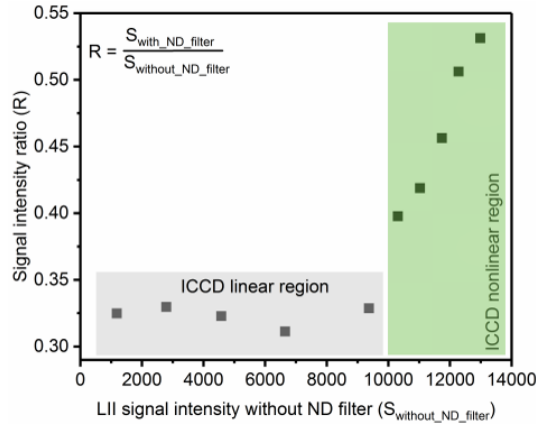


Figure S3: The linear and non-linear regions of ICCD. The ratio of flame LII signal intensity with a neutral density (ND) filter and without a ND filter is checked to rule out the ICCD linear region. Within the linear region, the signal intensity ratio should be a constant value. All the signals are confirmed to be within the ICCD linear region for the investigated flames.

### S1.2.2. Pressure effects on LII signals

The integrated LII signal over gate times of 0-90ns dropped by 28% from 2 to 5 bar and 12% from 5 to 15 bar, as shown in Fig. S5. The correction coefficients for pressure proposed by [1] were analyzed. It is determined that

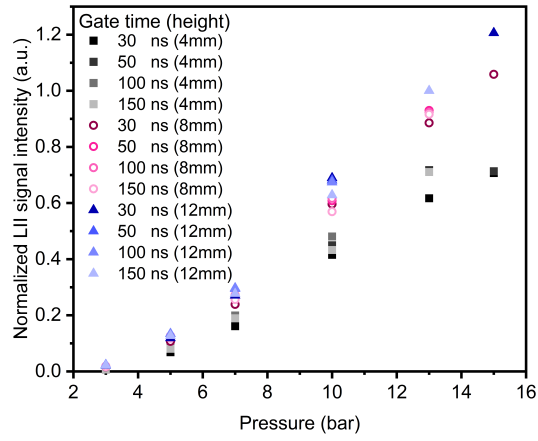


Figure S4: The LII signals at various gate times.

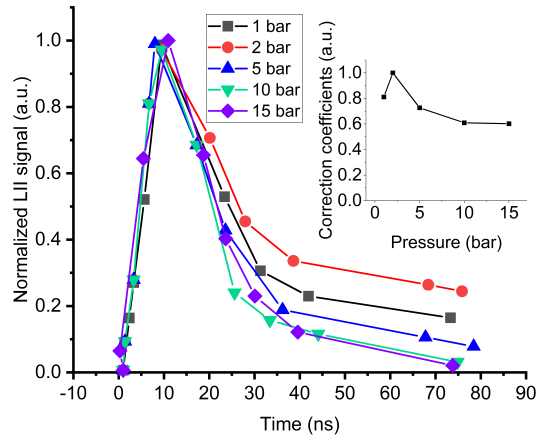


Figure S5: Temporal LII profiles. The subset shows the correction coefficients, which are the ratios of the integrated LII signals at 1, 5, 10, and 15 bar to that at 2 bar. The data was extracted from [1]

the linear correlation remained valid from 5 to 20 bar, the range of which is the focus of this study.

### S1.2.3. LIF signal selection

The LIF signal profiles for different heights of the laser sheet are presented in Fig. S6. The laser sheet was adjusted vertically, so that various portions of the laser sheet arrived to the flame. The LIF signals generated by different portions of laser sheet were scanned to obtain a uniform laser energy profile. In the present study,  $h = 30$  mm was used in the LIF measurement.

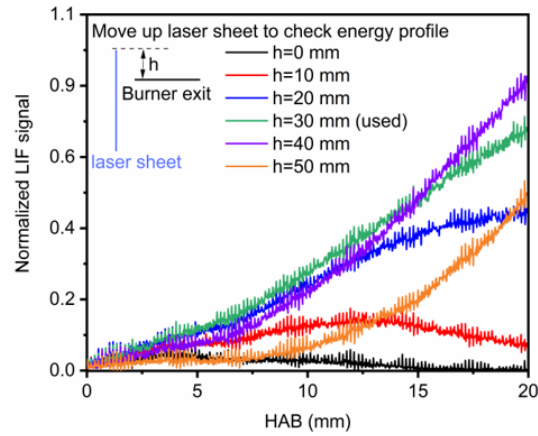


Figure S6: The LIF signal profiles for different heights of the laser sheet.

## S2. Varying parameters in CoFlame

The effects of varying  $\alpha$  and  $\gamma$  in the simulation of IDFs were assessed. The cases are listed in Table S1. Their comparisons of calculated  $f_v$ , HACA surface growth rates, and PAH adsorption rates at 10 bar are presented in Fig. S7, S8, and S9. It is found that the resultant  $f_v$ 's were not significantly affected by the variation in modeling parameters.

The effects of varying  $\alpha$  and  $\gamma$  on the mass contributions of different soot growth mechanisms are also shown in Fig. S10. For all cases, PAH adsorption remained the dominant mechanism of mass contribution, followed by HACA surface growth and soot inception. It is shown that varying  $\alpha$  and  $\gamma$  does not change the conclusion stated in the main text.

Table S1: Cases for sensitivity analysis.

| Case | $\alpha$ | $\gamma$ |
|------|----------|----------|
| 1    | 0.15     | 1.0      |
| 2    | 0.3      | 1.0      |
| 3    | 0.15     | 0.5      |

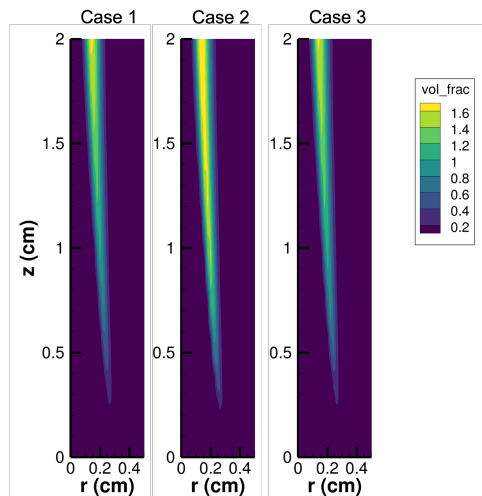


Figure S7: The 2D contour plots for soot volume fractions ( $f_v$ ) in the F70 flame at 10 bar. The unit is ppm.

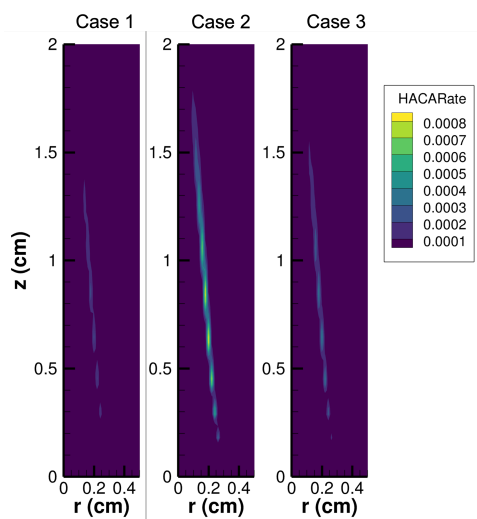


Figure S8: The 2D contour plots for the HACA surface growth rates in the F70 flame at 10 bar. The unit is  $\text{g cm}^{-3} \text{s}^{-1}$ .

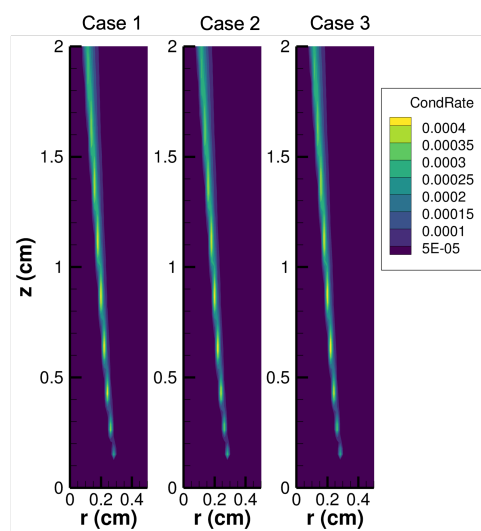


Figure S9: The 2D contour plots for the PAH adsorption rates in the F70 flame at 10 bar. The unit is  $\text{g cm}^{-3} \text{s}^{-1}$ .

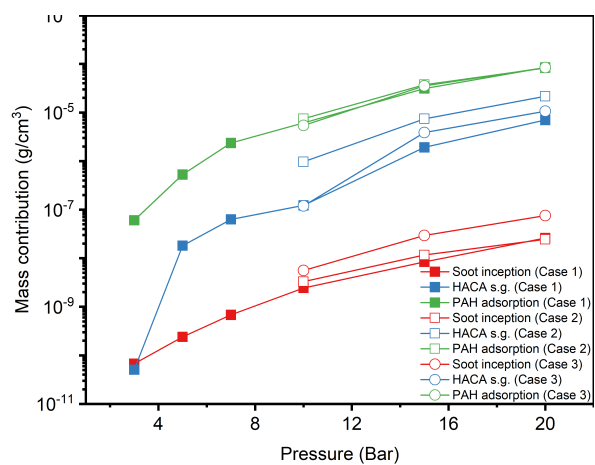


Figure S10: The mass contribution of PAH adsorption, HACA surface growth, and soot inception at various  $\alpha$  and  $\gamma$  values.

## References

- [1] M. Hofmann, W. G. Bessler, C. Schulz, H. Jander, Laser-induced incandescence for soot diagnostics at high pressures, *Applied optics* 42 (12) (2003) 2052–2062.